Journal of Magnetic Resonance **155,** 293–299 (2002)
doi:10.1006/jmre.2002.2519, available online at http://www.idealibrary.com on IDEAL®

COMMUNICATIONS

Sensitivity Enhancement in Structural Measurements by Solid State NMR through Pulsed Spin Locking

Aneta T. Petkova and Robert Tycko[1]

Laboratory of Chemical Physics, National Institutes of Diabetes and Digestive and Kidney Diseases, National Institutes of Health, Bethesda, Maryland 20892-0520

Received October 11, 2001; revised December 26, 2001

Free induction decay (FID) signals in solid state NMR measurements performed with magic angle spinning can often be extended in time by factors on the order of 10 by a simple pulsed spin locking technique. The sensitivity of a structural measurement in which the structural information is contained in the dependence of the integrated FID amplitude on a preceding evolution period can therefore be enhanced substantially by pulsed spin locking in the signal detection period. We demonstrate sensitivity enhancements in a variety of solid state NMR techniques that are applicable to selectively isotopically labeled samples, including ^{13}C–^{15}N rotational echo double resonance (REDOR), ^{13}C–^{13}C dipolar recoupling measurements using the constant-time finite-pulse radio-frequency-driven recoupling (fpRFDR-CT) and constant-time double-quantum-filtered dipolar recoupling (CTDQFD) techniques, and torsion angle measurements using the double quantum chemical shift anisotropy (DQCSA) technique. Further, we demonstrate that the structural information in the solid state NMR data is not distorted by pulsed spin locking in the detection period. © 2002 Elsevier Science (USA)

Key Words: **dipolar recoupling; REDOR; magic angle spinning; solid state NMR; pulsed spin locking; sensitivity enhancement.**

INTRODUCTION

A wide variety of solid state NMR techniques have been developed as experimental probes of the atomic-level structure of molecular solids. Often these techniques can provide structural information that is not available from other physical measurements, as in the cases of noncrystalline biological solids, synthetic polymers, and other complex noncrystalline molecular or network solids. Applications of these techniques are frequently limited by sensitivity considerations, with the requisite number of nuclei typically lying in the 0.1–1.0 μmole range for ^{13}C NMR measurements in a 9.4 T field at room temperature and with data acquisition times ranging from many hours to many days. Therefore, approaches to sensitivity enhancement in solid state NMR are of considerable current interest (*1–18*).

Many structural techniques such as dipolar recoupling measurements (*19–33*) or tensor correlation (*34–42*) measurements on selectively isotopically labeled compounds share a common feature that the structural information is contained in the dependence of integrated free induction decay (FID) signals on a preceding evolution period (e.g., a dipolar dephasing period), rather than in the direct time-dependence of the FID. In other words, the one-dimensional NMR spectrum or lineshape in the signal detection period is of little interest. In such cases, the sensitivity of the structural measurement can be enhanced by extending the FID using pulsed spin locking (*43–45*) (PSL) or a Carr–Purcell echo train (*46*). The utility of this approach to sensitivity enhancement has been appreciated and demonstrated previously in the context of multiple quantum NMR (MQNMR) of solids (*47, 48*), one-dimensional ^{13}C NMR spectroscopy of samples with inhomogeneously broadened lines under magic-angle spinning (MAS) (*49*), relaxation measurements on slowly-relaxing materials (*50, 51*), one-dimensional spectroscopy of half-integer quadrupolar nuclei in static powders (*52*), indirect detection of ^{13}C NMR spectra through ^{1}H NMR signals under MAS (*6*), and indirect detection of ^{14}N overtone NMR (*53–55*), ^{15}N NMR (*18*) and ^{2}H NMR (*17*) spectra in static solids. However, to our knowledge, the potential impact of PSL on the sensitivity of structural measurements based on heteronuclear and homonuclear dipolar recoupling techniques and tensor correlation techniques has not been explored, particularly in the case of measurements performed with MAS. We demonstrate this impact below by a series of experimental examples, performed under MAS at moderate (i.e., 5.0 kHz) or high (i.e., 20.0 kHz) frequencies, in which experimental data obtained with and without PSL are compared directly. Importantly, these examples also demonstrate that the structural information contained in the measurements is not significantly perturbed or distorted by PSL detection.

EXPERIMENTAL METHODS

NMR experiments were carried out at room temperature with Varian/Chemagnetics Infinity-400 spectrometers, operating at

[1] To whom correspondence should be addressed. E-mail: tycko@helix.nih.gov.

1090-7807/02 $35.00

^{13}C NMR frequencies of 100.4 and 100.8 MHz and with Varian/Chemagnetics magic angle spinning (MAS) probes with rotor diameters of 3.2 mm and 6 mm. ^{13}C-detected ^{13}C/^{15}N rotational echo double resonance (REDOR) experiments used the pulse sequence described by Anderson *et al.* (*56*), with 10.0 μs π pulses on both ^{13}C and ^{15}N nuclei and at a MAS frequency $\nu_R = 5.0$ kHz. Constant-time double-quantum-filtered dipolar recoupling (CTDQFD) experiments used the pulse sequence described by Bennett *et al.* (*34*), with a total radio-frequency-driven recoupling (*20, 26, 28*) (RFDR) period of $160\tau_R = 32.0$ ms (in the notation of reference (*34*), $L = 32$ and $M + N = 128$), where τ_R is the MAS rotor period, with 13.7 μs ^{13}C π pulses and $\nu_R = 5.0$ kHz. Double quantum chemical shift anisotropy (DQCSA) experiments used the pulse sequence described by Blanco and Tycko (*35*) in which three π pulses recouple the CSA interactions in the evolution period and with double quantum (DQ) excitation periods of $48\tau_R$ (pulse sequence in Fig. 2b of Ref. (*35*), with $n = 48$). ^{13}C π pulses in the RFDR train during the excitation periods were 13.7 μs, and $\nu_R = 5.0$ kHz. Constant-time finite-pulse radio-frequency-driven recoupling (fpRFDR-CT) experiments used the pulse sequence described by Ishii *et al.* (*57*), with a total fpRFDR evolution period of $768\tau_R$ and with two repetitions of the six-pulse WAHUHA cycle (in the notation of reference (*57*), $M + 2N = 384$ and $K = 2$). ^{13}C π pulses in the evolution period were 15.0 μs, and $\nu_R = 20.0$ kHz. In all experiments, ^{13}C π pulses in the dipolar recoupling periods were actively synchronized with an MAS tachometer signal. Proton decoupling fields during the recoupling periods were 120 kHz in REDOR and fpRFDR-CT experiments and 80 kHz in CTDQFD and DQCSA experiments. The ^{13}C carrier frequency was set to the middle of the NMR signals of interest in all PSL experiments, with the exception of the experiments for Fig. 7 where the dependence on resonance offset was explored deliberately.

As depicted in Fig. 1a, PSL trains consisted of N_P repetitions of the pulse sequence element τ_1–τ_2–P–τ_2–τ_1, where τ_1 represents a period during which N_S FID signal points were digitized with a dwell time t_d (25 μs in all measurements), τ_2 represents a dead time delay, and P represents a ^{13}C rf pulse with flip angle θ_P, length τ_P, and phase set to coincide with the direction of the ^{13}C magnetization of interest (i.e., to provide a spin locking field). Spin locking pulses were synchronized with MAS by adjusting the timing so that $2(\tau_1 + \tau_2) + \tau_P = k\tau_R$, with $k = 4$ in measurements at $\nu_R = 5.0$ kHz (i.e., REDOR, CTDQFD, and DQCSA) and $k = 20$ in measurements at $\nu_R = 20.0$ kHz (i.e., fpRFDR-CT). Following the digitization of $2N_PN_S$ signal points under PSL, an additional N_A signal points were acquired, again with dwell time t_d. Values of N_P and N_S are given in the figure captions. In all PSL experiments, $2N_PN_S + N_A = 2500$. The same number of data points was digitized in non-PSL experiments, with the same dwell time. The spectrometer's receiver bandwidth was set to approximately $1.3/t_d$ in experiments performed both with and without PSL. Proton decoupling fields during PSL were 70–85 kHz. Data processing included application of 20 Hz Gaussian line broadening to FIDs obtained with PSL. Line broadening of FIDs obtained without PSL was matched to the intrinsic linewidths to maximize the signal-to-noise ratio (SNR) in the spectrum. Total experiment times and all other conditions of data acquisition and processing were indentical in PSL and non-PSL versions of each measurement.

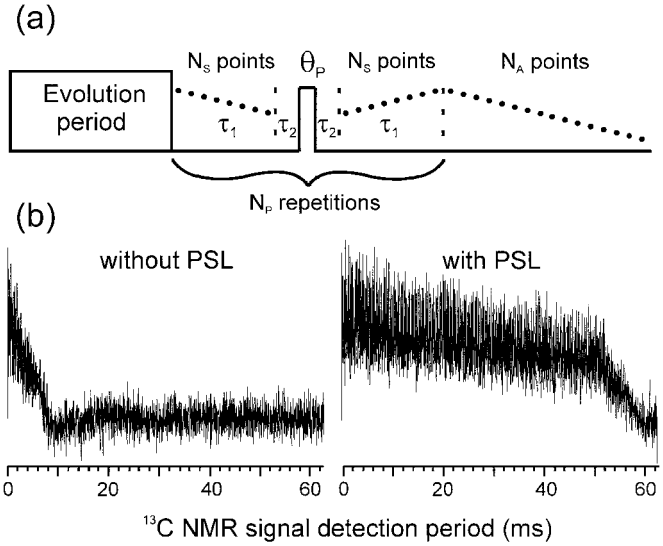

FIG. 1. (a) Schematic illustration of pulsed spin lock (PSL) detection in a structural measurement with magic-angle spinning (MAS) at frequency ν_R (rotor period τ_R). After an evolution period in which a pulse sequence for measuring dipole–dipole couplings or other structural parameters is applied, a train of N_P spin-locking pulses with flip angle θ_P and length τ_P is applied with a spacing of $k\tau_R$ between pulses, where k is an even integer. N_S signal points are digitized in each τ_1 period. Dead time periods are τ_2. N_A points are digitized at the end of the PSL train. (b) Experimental time-domain ^{13}C NMR signals from polycrystalline glycine-1-^{13}C,^{15}N (5% labeled molecules) at $\nu_R = 5.0$ kHz and an NMR frequency of 100.4 MHz, obtained with and without PSL. The rf carrier frequency is nearly on-resonance with the carboxylate signal. $N_P = 72$, $N_S = 14$, $N_A = 484$, $\theta_P = 180°$, $\tau_1 = 350.0$ μs, $\tau_2 = 45.0$ μs, and $\tau_P = 10.0$ μs.

Polycrystalline glycine in which 5% of the molecules were ^{15}N-labeled at the amine site and ^{13}C-labeled at the carboxyl site (glycine-1-^{13}C,^{15}N) was prepared by recrystallization of a mixture of labeled and unlabeled glycine. Polycrystalline Ala–Gly–Gly in which 3% of the molecules were ^{13}C-labeled at the carbonyl sites of Ala1 and Gly2 ($^{13}C_2$–AGG) was prepared as previously described (*58*). The peptide N–acetyl–Lys–Leu–Val–Phe–Phe–Ala–Glu–NH_2 (residues 16–22 of the Alzheimer's β-amyloid peptide, Aβ_{16-22}) was synthesized with a ^{13}C label at the carbonyl site of Leu17 and a ^{15}N label at the amide site of Ala21 and fibrillized as previously described (*59*). Polycrystalline L-alanine with a ^{13}C label at the carboxylate site (alanine-1-^{13}C) was used as received from Cambridge Isotopes Laboratories.

RESULTS

Figure 1b shows ^{13}C FID signals of glycine-1-^{13}C, ^{15}N obtained with and without PSL under conditions employed in the

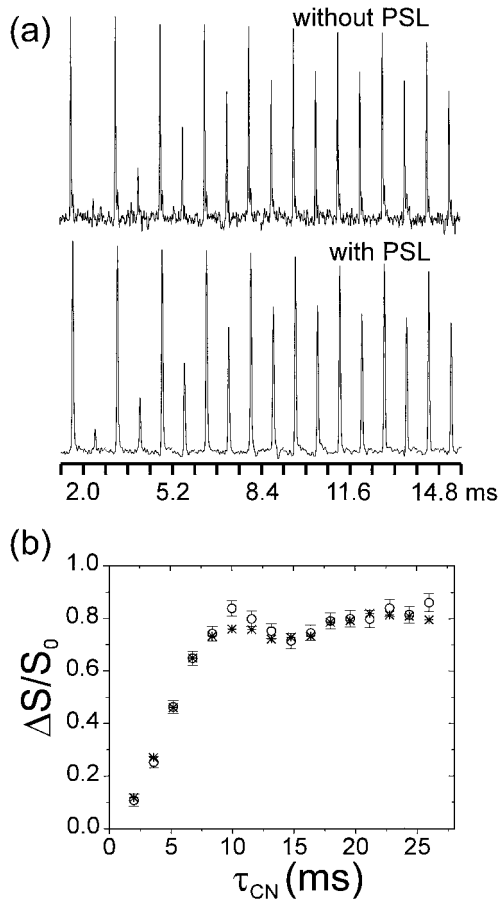

FIG. 2. ^{13}C-detected ^{13}C/^{15}N REDOR data for glycine-1-^{13}C,^{15}N (5% labeled molecules), obtained with the pulse sequence of Anderson *et al.* (*56*) (a) S_0 and ΔS REDOR spectra plotted alternately for increasing ^{13}C–^{15}N dephasing period τ_{CN}. Bottom is with PSL, showing 300 Hz spectral widths in each spectrum. Top is without PSL, showing 2000 Hz spectral widths in each spectrum. Data are acquired at 100.4 MHz, with $\nu_R = 5.0$ kHz, $N_P = 72$, $N_S = 14$, $N_A = 484$, $\theta_P = 180^\circ$, $\tau_1 = 350.0\ \mu$s, $\tau_2 = 45.0\ \mu$s, and $\tau_P = 10.0\ \mu$s. Total of 36 scans in each REDOR data set. (b) REDOR build-up curves measured with (asterisks) and without (open circles) PSL. Error bars shown for data without PSL represent uncertainty derived from the root-mean-squared noise in the experimental spectra. Corresponding uncertainty for data with PSL is about equal to the size of the symbols.

REDOR experiments. PSL clearly extends the FID signals substantially, in this case by a factor of six or more. Figure 2 compares REDOR data obtained with and without PSL. The SNR of the data is enhanced by PSL. Good agreement between REDOR build-up curves obtained with and without PSL is found, indicating that the internuclear distance information in the REDOR measurement is not distorted by PSL detection. In these experiments $\theta_P = 180^\circ$, so that the PSL train was identical to a rotor-synchronized Carr–Purcell echo train. For glycine-1-^{13}C, ^{15}N, a sample in which ^{13}C–^{13}C dipole–dipole couplings are negligibly small, the effectiveness of PSL is insensitive to θ_P over a broad range around 180°.

Figure 3 compares CTDQFD data for $^{13}C_2$–AGG obtained with and without PSL. Figure 3a shows that the resolved NMR lines of the two labeled carbonyl carbons in the DQ-filtered MAS spectrum are collapsed to a single, sharper line by PSL and the spinning sideband lines are split due to amplitude modulation of the FID signals imposed by PSL. The observed splitting depends on the separation between PSL pulses and the dead time in the PSL train. Figure 3b shows that the CTDQFD dephasing curve, which contains information about the peptide conformation (*34*), is not affected significantly by PSL. CTDQFD data points in Fig. 3b were obtained by summing the areas of centerband and first-order sideband signals in the non-PSL spectra or by summing the centerband and the four most intense sideband signals (at ±4.285 kHz and ±5.715 kHz). Similar summations were used to generate the data points in Figs. 2b and 4a.

Figure 4a compares DQCSA data for $^{13}C_2$-AGG obtained with and without PSL. The DQCSA evolution curve, which contains information about the peptide conformation (*35*), is not affected significantly by PSL. Figure 4b shows the dependence of the centerband lineshape for $^{13}C_2$-AGG under PSL

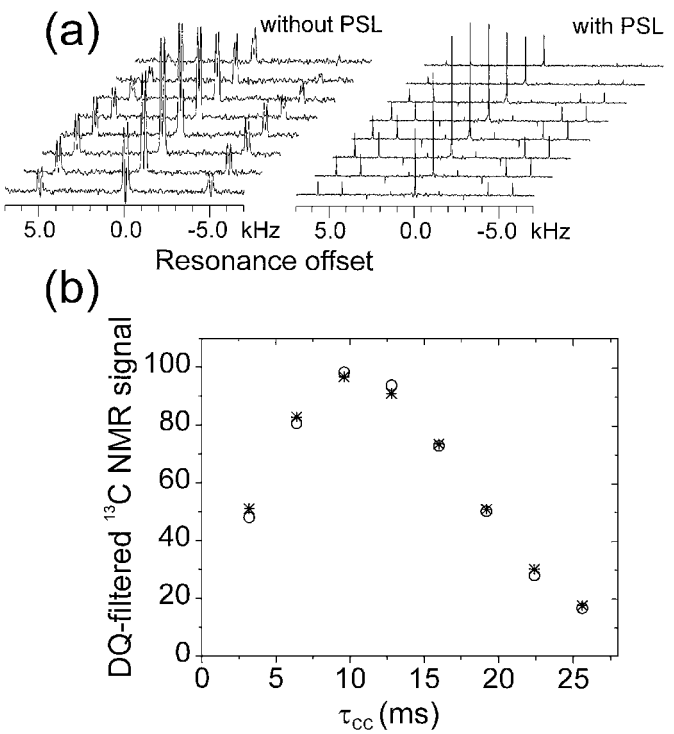

FIG. 3. Constant-time double-quantum-filtered dipolar recoupling (CT-DQFD) data for polycrystalline $^{13}C_2$–AGG (3% labeled molecules), obtained with the pulse sequence of Bennett *et al.* (*34*) (a) DQ-filtered ^{13}C NMR spectra obtained at ^{13}C–^{13}C evolution times τ_{CC} from 3.2 ms to 25.6 ms in increments of 3.2 ms. Left is without PSL. Right is with PSL, showing the apparent splitting of spinning sideband lines due to amplitude modulation of the time-domain signals imposed by PSL. Data are acquired at 100.8 MHz, with $\nu_R = 5.0$ kHz, $N_P = 80$, $N_S = 14$, $N_A = 260$, $\theta_P = 162^\circ$, $\tau_1 = 350.0\ \mu$s, $\tau_2 = 45.5\ \mu$s, and $\tau_P = 9.0\ \mu$s. (b) CTDQFD dephasing curves measured with (asterisks) and without (open circles) PSL. Uncertainty due to noise in the experimental spectra is about equal to the size of the symbols: total of 1024 scans in each CTDQFD data set.

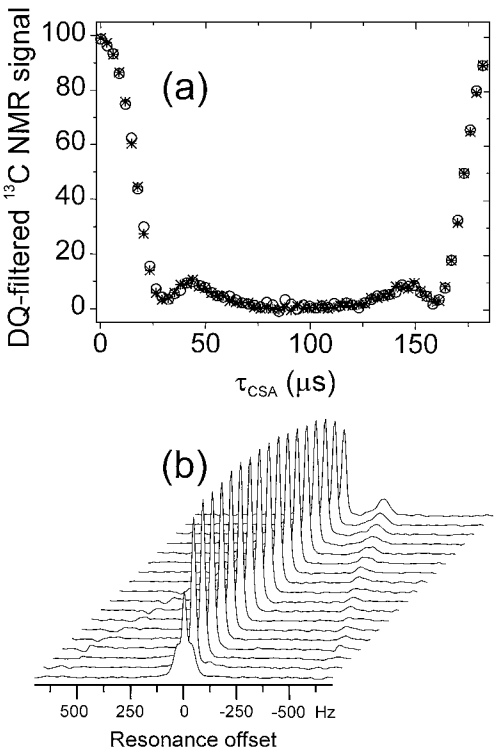

FIG. 4. (a) Double quantum chemical shift anisotropy (DQCSA) curves for $^{13}C_2$-AGG (3% labeled molecules), obtained with the pulse sequence of Blanco and Tycko (*35*). ^{13}C NMR signals are detected with (asterisks) and without (open circles) PSL. Uncertainty due to noise in the experimental spectra is less than the size of the symbols. Data are acquired at 100.8 MHz, with $\nu_R = 5.0$ kHz, $N_P = 80$, $N_S = 14$, $N_A = 260$, $\theta_P = 162^\circ$, $\tau_1 = 350.0$ μs, $\tau_2 = 45.5$ μs, and $\tau_P = 9.0$ μs: total of 16384 scans in each DQCSA data set. (b) Dependence of the spin-locked centerband ^{13}C NMR lineshape for $^{13}C_2$-AGG on θ_P for a constant ^{13}C rf amplitude of 50 kHz. Values of θ_P range from 180° (lowest spectrum) to 27° in decrements of 9°.

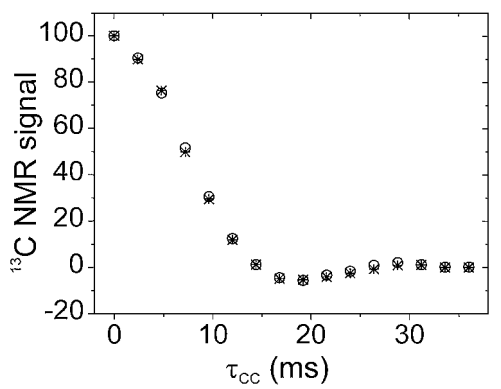

FIG. 5. Constant-time finite-pulse radio-frequency-driven recoupling (fpRFDR-CT) curves for polycrystalline L-alanine-1-^{13}C (99% labeled molecules), obtained with the pulse sequence of Ishii *et al.* (*57*) ^{13}C NMR signals are detected with (asterisks) and without (open circles) PSL. τ_{CC} is the effective ^{13}C–^{13}C dipolar dephasing period. Uncertainty due to noise in the experimental spectra is less than the size of the symbols. Data are acquired at 100.4 MHz, with $\nu_R = 20.0$ kHz, $N_P = 52$, $N_S = 18$, $N_A = 628$, $\theta_P = 180^\circ$, $\tau_1 = 450.0$ μs, $\tau_2 = 45.0$ μs, and $\tau_P = 10.0$ μs: total of 32 scans in each fpRFDR-CT data set.

on θ_P. For $^{13}C_2$-AGG, the relatively strong ^{13}C–^{13}C couplings (3.2 Å internuclear distance) lead to significant broadening of the PSL lineshape at $\theta_P \approx 180^\circ$, presumably through an RFDR recoupling mechanism. At $\theta_P \leq 120^\circ$, significant splitting of the centerband lineshape is observed. Optimal values of θ_P at moderate MAS frequencies appear to be in the 130–160° range for samples with significant homonuclear couplings.

Figure 5 compares fpRFDR-CT data for alanine-1-^{13}C obtained with and without PSL. The fpRFDR-CT dephasing curve reflects internuclear distances (*57*). Again, the experimental curve is not affected by PSL. The fpRFDR-CT data are acquired at $\nu_R = 20.0$ kHz, indicating that sensitivity enhancements can be obtained without degradation of structural information even at high MAS frequencies.

DISCUSSION

The improvement in SNR brought about by PSL is $\xi = [(m_0\Delta_0)/(m_{PSL}\Delta_{PSL})]^{1/2}$, where Δ_0 and m_0 are the linewidth and number of summed sidebands without PSL, and Δ_{PSL} and m_{PSL} are the apparent linewidth and number of summed sidebands with PSL. This expression assumes matched filtering, identical lineshapes with and without PSL, and identical numbers of scans. Of course, the data acquisition time required to achieve a specified SNR scales as ξ^2, assuming a fixed repetition rate for signal averaging. As an example, $\xi^2 \approx 4$ for the REDOR data in Fig. 2. While this value is already significant, it represents an underestimate of the sensitivity enhancements expected in many measurements on samples that are of genuine interest in chemistry, physics, materials science, and structural biology. Most samples that are not polycrystalline compounds exhibit substantial inhomogeneous broadening from structural disorder, either conformational disorder of the molecule of interest or disorder of the surrounding matrix. This inhomogeneous broadening typically increases ^{13}C MAS NMR linewidths Δ_0 to the 1.5–6 ppm range but does not affect Δ_{PSL}. Thus, values of ξ^2 ranging from 7 to 30 are expected for typical noncrystalline samples at a field of 9.4 T.

As an illustration of the sensitivity enhancement achievable in structural measurements on noncrystalline compounds of biological interest, Fig. 6 compares REDOR data obtained for amyloid fibrils formed by the peptide Aβ_{16-22} with and without PSL. REDOR measurements on this sample have previously shown that the β-sheets in Aβ_{16-22} fibrils have an antiparallel structure (*59*). In this case, $\xi^2 \approx 12$, corresponding to a reduction in ^{13}C linewidth from 250 Hz to 20 Hz.

The most significant drawback of PSL is the loss of spectral resolution in the directly detected dimension of a structural measurement. In the experimental examples given above, in which samples are ^{13}C-labeled at specific sites, spectral resolution in the directly detected dimension carries no important information. However, in samples with multiple ^{13}C-labeled sites or with relatively large natural abundance ^{13}C NMR signals, the

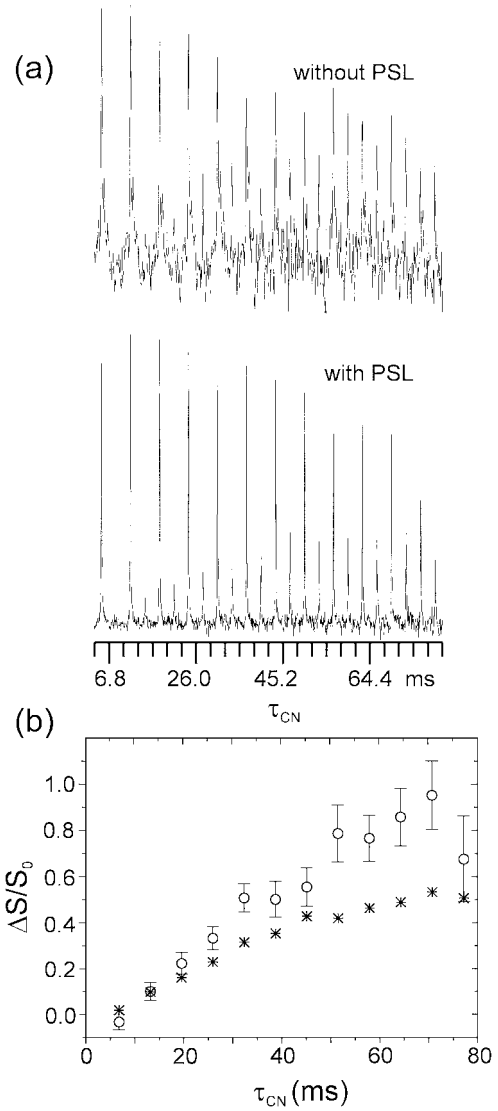

FIG. 6. (a) ^{13}C-detected ^{13}C/^{15}N REDOR data for Aβ_{16-22} amyloid fibrils, ^{13}C-labeled at the carbonyl site of Leu17 and ^{15}N-labeled at the amide site of Ala21. S_0 and ΔS REDOR spectra are plotted alternately for increasing ^{13}C–^{15}N dephasing period τ_{CN}: top is without PSL; bottom is with PSL. Data are acquired at 100.4 MHz, with $\nu_R = 5.0$ kHz, $N_P = 72$, $N_S = 14$, $N_A = 484$, $\theta_P = 180^\circ$, $\tau_1 = 350.0$ μs, $\tau_2 = 45.0$ μs, and $\tau_P = 10.0$ μs: total experiment times were 4.25 h for each complete data set, with a recycle delay of 4 s and approximately 2 mg (2 μmol) of labeled sample. (b) REDOR build-up curves for data obtained with PSL (asterisks) and without PSL (open circles). Error bars shown for data without PSL represent uncertainty derived from the root-mean-squared noise in the experimental spectra. Corresponding uncertainty for data with PSL is about equal to the size of the symbols. The two build-up curves agree to within the experimental noise, except that all $\Delta S/S_0$ values measured with PSL are reduced by a factor of approximately 0.67 due to spin-locked ^{13}C background signals (see text).

loss of spectral resolution may complicate the data analysis. For example, in a ^{13}C-detected ^{13}C/^{15}N REDOR measurement, loss of resolution between ^{13}C signals from the labeled site of interest (coupled to ^{15}N) and extraneous signals (not coupled to ^{15}N) leads to a reduction in the experimental $\Delta S/S_0$ values that may be difficult to calibrate unless the REDOR build-up curve is measured to large enough values of the dephasing time τ_{CN} that the asymptotic value of $\Delta S/S_0$ can be determined. For example, if the REDOR data in Fig. 6 were recorded only to $\tau_{CN} \leq 45$ ms, an accurate distance determination would not be possible. Recording data at larger values of τ_{CN} allows the scale of the $\Delta S/S_0$ values to be determined experimentally.

Complications due to spin-locked background signals may be ameliorated in measurements that employ DQ filtering (*60, 61*), difference spectroscopy (*62*), or other methods of signal selection. In addition, extraneous NMR signals at resonance offsets greater than $(k\tau_R)^{-1}$ contribute principally to sideband signals in the Fourier transform of the PSL FID, while on-resonance signals contribute principally to the centerband. Figure 7 shows the experimental dependence of the centerband signal amplitude on resonance offset. Thus, some degree of spectral resolution may be retained, depending on the timing parameters and carrier frequency of the PSL sequence, sufficient to minimize the contributions to the data from background signals that are far off-resonance.

The experiments reported above were carried out on samples in which the ^{13}C signals of interest have a single isotropic shift (Figs. 2, 5, and 6) or a small isotropic shift difference (Figs. 3 and 4). When the isotropic shift differences are large compared with $(k\tau_R)^{-1}$, all signals will not be collapsed into the PSL centerband signal. Thus, in a dipolar recoupling measurement that depends on large isotropic shift differences (*25*) or is applied to systems with large isotropic shift differences (*20, 26, 28*), it may be necessary to record PSL FIDs for the different ^{13}C sites separately with different rf carrier frequencies, or to analyze the PSL sideband signals if a single carrier frequency is used.

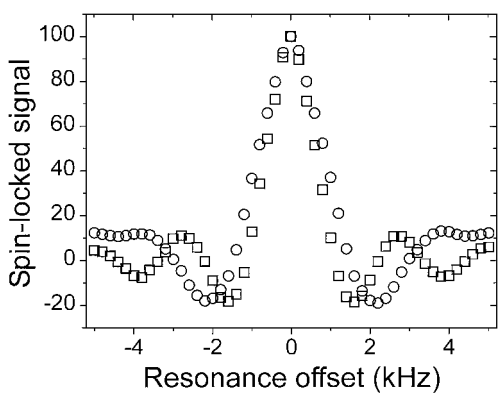

FIG. 7. Dependence of the area of the spin-locked centerband signal from L-alanine-1-^{13}C on the frequency offset of the rf carrier from the carboxylate ^{13}C NMR line. Data are shown for $\nu_R = 20.0$ kHz (open squares, $N_P = 52$, $N_S = 18$, $N_A = 628$, $\theta_P = 150^\circ$, $\tau_1 = 450.0$ μs, $\tau_2 = 42.5$ μs, and $\tau_P = 15.0$ μs) and $\nu_R = 5.0$ kHz (open circles, $N_P = 72$, $N_S = 14$, $N_A = 484$, $\theta_P = 150^\circ$, $\tau_1 = 350.0$ μs, $\tau_2 = 45.0$ μs, and $\tau_P = 10.0$ μs).

The labeled ^{13}C sites in the experiments reported have no directly bonded protons. Similar results are expected for sites with directly bonded protons, although higher proton decoupling fields may be required to achieve the 20 Hz PSL linewidths achieved in our experiments. Although our experiments to date have been performed at 9.4 T, the PSL technique is not limited to this specific field value.

In conclusion, we have demonstrated experimentally that significant sensitivity enhancements can be achieved through PSL in solid state NMR measurements of the type that are widely used in structural measurements. PSL detection has the potential to make solid state NMR measurements possible that would otherwise be precluded by the lack of sufficient sample quantities. We anticipate future applications and extensions of PSL detection, particularly in NMR measurements on noncrystalline biological solids such as membrane proteins, high molecular weight complexes in frozen solution, and amyloid fibrils.

ACKNOWLEDGMENTS

We thank James P. Yesinowski for discussions that stimulated this work and John J. Balbach for providing the Aβ_{16-22} amyloid fibril sample used in experiments in Fig. 6. This work was supported in part by a grant from the Intramural AIDS Targeted Antiviral Program of the National Institutes of Health.

REFERENCES

1. R. Tycko, S. E. Barrett, G. Dabbagh, L. N. Pfeiffer, and K. W. West, Electronic states in gallium arsenide quantum wells probed by optically pumped NMR, *Science* **268,** 1460–1463 (1995).
2. S. E. Barrett, G. Dabbagh, L. N. Pfeiffer, K. W. West, and R. Tycko, Optically pumped NMR evidence for finite-size skyrmions in GaAs quantum wells near landau-level filling $\nu = 1$, *Phys. Rev. Lett.* **74,** 5112–5115 (1995).
3. R. Tycko, Optical pumping in indium phosphide: ^{13}P NMR measurements and potential for signal enhancement in biological solid state NMR, *Solid State Nucl. Magn. Reson.* **11,** 1–9 (1998).
4. C. A. Michal and R. Tycko, Nuclear spin polarization transfer with a single radio-frequency field in optically pumped indium phosphide, *Phys. Rev. Lett.* **81,** 3988–3991 (1998).
5. Y. Ishii and R. Tycko, Sensitivity enhancement in solid state ^{15}N NMR by indirect detection with high-speed magic angle spinning, *J. Magn. Reson.* **142,** 199–204 (2000).
6. Y. Ishii, J. P. Yesinowski, and R. Tycko, Sensitivity enhancement in solid-state ^{13}C NMR of synthetic polymers and biopolymers by ^{1}H NMR detection with high-speed magic angle spinning, *J. Am. Chem. Soc.* **123,** 2921–2922 (2001).
7. D. A. Hall, D. C. Maus, G. J. Gerfen, S. J. Inati, L. R. Becerra, F. W. Dahlquist, and R. G. Griffin, Polarization-enhanced NMR spectroscopy of biomolecules in frozen solution, *Science* **276,** 930–932 (1997).
8. M. Rosay, A. C. Zeri, N. S. Astrof, S. J. Opella, J. Herzfeld, and R. G. Griffin, Sensitivity-enhanced NMR of biological solids: Dynamic nuclear polarization of Y21M fd bacteriophage and purple membrane, *J. Am. Chem. Soc.* **123,** 1010–1011 (2001).
9. M. Afeworki, R. A. McKay, and J. Schaefer, Selective observation of the interface of heterogeneous polycarbonate polystyrene blends by dynamic nuclear polarization ^{13}C NMR spectroscopy, *Macromolecules* **25,** 4084–4091 (1992).
10. M. Afeworki, S. Vega, and J. Schaefer, Direct electron-to-carbon polarization transfer in homogeneously doped polycarbonates, *Macromolecules* **25,** 4100–4105 (1992).
11. H. Lock, R. A. Wind, G. E. Maciel, and C. E. Johnson, A study of ^{13}C-enriched chemical vapor deposited diamond film by means of ^{13}C nuclear magnetic resonance, electron paramagnetic resonance, and dynamic nuclear polarization, *J. Chem. Phys.* **99,** 3363–3379 (1993).
12. J. Z. Hu, J. W. Zhou, B. L. Yang, L. Y. Li, J. Q. Qiu, C. H. Ye, M. S. Solum, R. A. Wind, R. J. Pugmire, and D. M. Grant, Dynamic nuclear polarization of nitrogen-15 in benzamide, *Solid State Nucl. Magn. Reson.* **8,** 129–137 (1997).
13. J. Z. Hu, M. S. Solum, R. A. Wind, B. L. Nilsson, M. A. Peterson, R. J. Pugmire, and D. M. Grant, ^{1}H and ^{15}N dynamic nuclear polarization studies of carbazole, *J. Phys. Chem. A* **104,** 4413–4420 (2000).
14. G. G. Maresch, R. D. Kendrick, C. S. Yannoni, and M. E. Galvin, Interfacial electron nuclear polarization transfer in polymer composites, *Macromolecules* **21,** 3523–3525 (1988).
15. G. G. Maresch, R. D. Kendrick, C. S. Yannoni, and M. E. Galvin, Dynamic nuclear polarization via confined electrons in bulk solids, *J. Magn. Reson.* **82,** 41–50 (1989).
16. I. Schnell, B. Langer, S. H. M. Sontjens, M. H. P. van Genderen, R. P. Sijbesma, and H. W. Spiess, Inverse detection and heteronuclear editing in ^{1}H-^{15}N correlation and ^{1}H-^{1}H double-quantum NMR spectroscopy in the solid state under fast MAS, *J. Magn. Reson.* **150,** 57–70 (2001).
17. K. Schmidt-Rohr, K. Saalwachter, S. F. Liu, and M. Hong, High-sensitivity ^{2}H NMR in solids by ^{1}H detection, *J. Am. Chem. Soc.* **123,** 7168–7169 (2001).
18. M. Hong and S. Yamaguchi, Sensitivity-enhanced static ^{15}N NMR of solids by ^{1}H indirect detection, *J. Magn. Reson.* **150,** 43–48 (2001).
19. T. Gullion and J. Schaefer, Rotational echo double resonance NMR, *J. Magn. Reson.* **81,** 196–200 (1989).
20. T. Gullion and S. Vega, A simple magic angle spinning NMR experiment for the dephasing of rotational echoes of dipolar coupled homonuclear spin pairs, *Chem. Phys. Lett.* **194,** 423–428 (1992).
21. R. Tycko and G. Dabbagh, Measurement of nuclear magnetic dipole–dipole couplings in magic angle spinning NMR, *Chem. Phys. Lett.* **173,** 461–465 (1990).
22. R. Tycko and G. Dabbagh, Double-quantum filtering in magic-angle-spinning NMR spectroscopy: An approach to spectral simplification and molecular structure determination, *J. Am. Chem. Soc.* **113,** 9444–9448 (1991).
23. R. Tycko and S. O. Smith, Symmetry principles in the design of pulse sequences for structural measurements in magic angle spinning nuclear magnetic resonance, *J. Chem. Phys.* **98,** 932–943 (1993).
24. R. Tycko, Normal angle spinning dipolar spectroscopy for structural studies by solid-state nuclear magnetic resonance, *J. Am. Chem. Soc.* **116,** 2217–2218 (1994).
25. D. P. Raleigh, M. H. Levitt, and R. G. Griffin, Rotational resonance in solid state NMR, *Chem. Phys. Lett.* **146,** 71–76 (1988).
26. A. E. Bennett, J. H. Ok, R. G. Griffin, and S. Vega, Chemical shift correlation spectroscopy in rotating solids: radio frequency driven dipolar recoupling and longitudinal exchange, *J. Chem. Phys.* **96,** 8624–8627 (1992).
27. C. M. Rienstra, M. E. Hatcher, L. J. Mueller, B. Q. Sun, S. W. Fesik, and R. G. Griffin, Efficient multispin homonuclear double-quantum recoupling for magic-angle spinning NMR: ^{13}C–^{13}C correlation spectroscopy of U-^{13}C-erythromycin A, *J. Am. Chem. Soc.* **120,** 10,602–10,612 (1998).
28. A. E. Bennett, C. M. Rienstra, J. M. Griffiths, W. G. Zhen, P. T. Lansbury, and R. G. Griffin, Homonuclear radio frequency driven recoupling in rotating solids, *J. Chem. Phys.* **108,** 9463–9479 (1998).

29. M. Hohwy, C. M. Rienstra, C. P. Jaroniec, and R. G. Griffin, Fivefold symmetric homonuclear dipolar recoupling in rotating solids: Application to double quantum spectroscopy, *J. Chem. Phys.* **110,** 7983–7992 (1999).

30. D. M. Gregory, D. J. Mitchell, J. A. Stringer, S. Kiihne, J. C. Shiels, J. Callahan, M. A. Mehta, and G. P. Drobny, Windowless dipolar recoupling: The detection of weak dipolar couplings between spin-1/2 nuclei with large chemical shift anisotropies, *Chem. Phys. Lett.* **246,** 654–663 (1995).

31. Y. K. Lee, N. D. Kurur, M. Helmle, O. G. Johannessen, N. C. Nielsen, and M. H. Levitt, Efficient dipolar recoupling in the NMR of rotating solids: A sevenfold symmetrical radiofrequency pulse sequence, *Chem. Phys. Lett.* **242,** 304–309 (1995).

32. M. Hohwy, H. J. Jakobsen, M. Eden, M. H. Levitt, and N. C. Nielsen, Broadband dipolar recoupling in the nuclear magnetic resonance of rotating solids: A compensated C7 pulse sequence, *J. Chem. Phys.* **108,** 2686–2694 (1998).

33. R. Verel, M. Ernst, and B. H. Meier, Adiabatic dipolar recoupling in solid-state NMR: The DREAM scheme, *J. Magn. Reson.* **150,** 81–99 (2001).

34. A. E. Bennett, D. P. Weliky, and R. Tycko, Quantitative conformational measurements in solid state NMR by constant-time homonuclear dipolar recoupling, *J. Am. Chem. Soc.* **120,** 4897–4898 (1998).

35. F. J. Blanco and R. Tycko, Determination of polypeptide backbone dihedral angles in solid state NMR by double quantum ^{13}C chemical shift anisotropy measurements, *J. Magn. Reson.* **149,** 131–138 (2001).

36. X. Feng, Y. K. Lee, D. Sandstrom, M. Eden, H. Maisel, A. Sebald, and M. H. Levitt, Direct determination of a molecular torsional angle by solid-state NMR, *Chem. Phys. Lett.* **257,** 314–320 (1996).

37. X. Feng, M. Eden, A. Brinkmann, H. Luthman, L. Eriksson, A. Graslund, O. N. Antzutkin, and M. H. Levitt, Direct determination of a peptide torsional angle ψ by double-quantum solid-state NMR, *J. Am. Chem. Soc.* **119,** 12,006–12,007 (1997).

38. P. R. Costa, J. D. Gross, M. Hong, and R. G. Griffin, Solid-state NMR measurement of ψ in peptides: A NCCN 2Q-heteronuclear local field experiment, *Chem. Phys. Lett.* **280,** 95–103 (1997).

39. M. Hong, J. D. Gross, and R. G. Griffin, Site-resolved determination of peptide torsion angle ϕ from the relative orientations of backbone N-H and C-H bonds by solid-state NMR, *J. Phys. Chem. B* **101,** 5869–5874 (1997).

40. M. Hong, J. D. Gross, W. Hu, and R. G. Griffin, Determination of the peptide torsion angle ϕ by ^{15}N chemical shift and $^{13}C_\alpha$–$^{1}H_\alpha$ dipolar tensor correlation in solid-state MAS NMR, *J. Magn. Reson.* **135,** 169–177 (1998).

41. B. Reif, M. Hohwy, C. P. Jaroniec, C. M. Rienstra, and R. G. Griffin, NH-NH vector correlation in peptides by solid-state NMR, *J. Magn. Reson.* **145,** 132–141 (2000).

42. P. V. Bower, N. Oyler, M. A. Mehta, J. R. Long, P. S. Stayton, and G. P. Drobny, Determination of torsion angles in proteins and peptides using solid state NMR, *J. Am. Chem. Soc.* **121,** 8373–8375 (1999).

43. E. D. Ostroff and J. S. Waugh, Multiple spin echoes and spin locking in solids, *Phys. Rev. Lett.* **16,** 1097–1098 (1966).

44. W.-K. Rhim, D. P. Burum, and D. D. Elleman, Multiple-pulse spin locking in dipolar solids, *Phys. Rev. Lett.* **37,** 1764–1766 (1976).

45. D. Suwelack and J. S. Waugh, Quasistationary magnetization in pulsed spin-locking experiments in dipolar solids, *Phys. Rev. B—Condens. Matter* **22,** 5110–5114 (1980).

46. H. Y. Carr and E. M. Purcell, Effects of diffusion on free precession in nuclear magnetic resonance experiments, *Phys. Rev.* **94,** 630–638 (1954).

47. D. P. Weitekamp, Time-domain multiple-quantum NMR, *Adv. Magn. Reson.* **11,** 111–274 (1983).

48. J. Baum and A. Pines, NMR studies of clustering in solids, *J. Am. Chem. Soc.* **108,** 7447–7454 (1986).

49. P. M. Henrichs and V. A. Nicely, ^{13}C NMR study of the conformation and dynamics of bisphenol A polycarbonate, *Macromolecules* **24,** 2506–2513 (1991).

50. S. E. Barrett, J. A. Martindale, D. J. Durand, C. H. Pennington, C. P. Slichter, T. A. Friedmann, J. P. Rice, and D. M. Ginsberg, Anomalous behavior of nuclear spin–lattice relaxation rates in $YBa_2Cu_3O_7$ below T_c, *Phys. Rev. Lett.* **66,** 108–111 (1991).

51. R. Tycko, G. Dabbagh, M. J. Rosseinsky, D. W. Murphy, A. P. Ramirez, and R. M. Fleming, Electronic properties of normal and superconducting alkali fullerides probed by ^{13}C nuclear magnetic resonance, *Phys. Rev. Lett.* **68,** 1912–1915 (1992).

52. F. H. Larsen, H. J. Jakobsen, P. D. Ellis, and N. C. Nielsen, Sensitivity-enhanced quadrupolar-echo NMR of half-integer quadrupolar nuclei. Magnitudes and relative orientations of chemical shielding and quadrupolar coupling tensors, *J. Phys. Chem. A* **101,** 8597–8606 (1997).

53. R. Tycko and S. J. Opella, High-resolution ^{14}N overtone spectroscopy: An approach to natural abundance nitrogen NMR of oriented and polycrystalline systems, *J. Am. Chem. Soc.* **108,** 3531–3532 (1986).

54. R. Tycko and S. J. Opella, Overtone NMR spectroscopy, *J. Chem. Phys.* **86,** 1761–1774 (1987).

55. A. N. Garroway and J. B. Miller, Demonstration of indirect detection of ^{14}N $\Delta m = 2$ (overtone) NMR transitions, *J. Magn. Reson.* **82,** 591–596 (1989).

56. R. C. Anderson, T. Gullion, J. M. Joers, M. Shapiro, E. B. Villhauer, and H. P. Weber, Conformation of [1-^{13}C,^{15}N]acetyl-L-carnitine: Rotational echo double resonance nuclear magnetic resonance spectroscopy, *J. Am. Chem. Soc.* **117,** 10,546–10,550 (1995).

57. Y. Ishii, J. J. Balbach, and R. Tycko, Measurement of dipole-coupled lineshapes in a many-spin system by constant-time two-dimensional solid state NMR with high-speed magic-angle spinning, *Chem. Phys.* **266,** 231–236 (2001).

58. R. Tycko, D. P. Weliky, and A. E. Berger, Investigation of molecular structure in solids by two-dimensional NMR exchange spectroscopy with magic angle spinning, *J. Chem. Phys.* **105,** 7915–7930 (1996).

59. J. J. Balbach, Y. Ishii, O. N. Antzutkin, R. D. Leapman, N. W. Rizzo, F. Dyda, J. Reed, and R. Tycko, Amyloid fibril formation by $A\beta_{16\text{-}22}$, a seven-residue fragment of the Alzheimer's β-amyloid peptide, and structural characterization by solid state NMR, *Biochemistry* **39,** 13,748–13,759 (2000).

60. D. P. Weliky, A. E. Bennett, A. Zvi, J. Anglister, P. J. Steinbach, and R. Tycko, Solid-state NMR evidence for an antibody-dependent conformation of the V3 loop of HIV-1 gp120, *Nat. Struct. Biol.* **6,** 141–145 (1999).

61. F. J. Blanco, S. Hess, L. K. Pannell, N. W. Rizzo, and R. Tycko, Solid-state NMR data support a helix-loop-helix structural model for the N-terminal half of HIV-1 Rev in fibrillar form, *J. Molec. Biol.* **313,** 845–859 (2001).

62. H. J. M. Degroot, V. Copie, S. O. Smith, P. J. Allen, C. Winkel, J. Lugtenburg, J. Herzfeld, and R. G. Griffin, Magic angle sample spinning NMR difference spectroscopy, *J. Magn. Reson.* **77,** 251–257 (1988).